Science
AAAS

Synthesis and Measurement of Ultrafast Waveforms from Five Discrete Optical Harmonics

Han-Sung Chan *et al.*

Science **331**, 1165 (2011);
DOI: 10.1126/science.1198397

Science (print ISSN 0036-8075; online ISSN 1095-9203) is published weekly, except the last week in December, by the American Association for the Advancement of Science, 1200 New York Avenue NW, Washington, DC 20005.

conformation found in our crystal structure (Fig. 6B). Generating a two-head-bound microtubule intermediate cannot be achieved simply by a rotation around the GST-linker boundary. Moreover, the possible ways to position the two heads on the microtubule are constrained by a "short leash" between the GST and the motor domains (Fig. 1B). However, we could dock the second head to the microtubule and create a two-head-bound intermediate by rotating the motor ring, detaching the linker, and altering the stalk (Fig. 6B, right). In this tentative model, the MTBDs are bound to neighboring protofilaments of the microtubule, with one MTBD positioned 8 nm in front of the other (Fig. 6B). The front head with the detached linker is in a pre-powerstroke state, and the rear head with the docked linker is in a post-powerstroke state (*7*, *8*), which is similar to the conformation of the mechanical elements of kinesin and myosin in their two-head-bound intermediate state (*38*, *39*).

The two-head-bound model shown in Fig. 6B raises questions of how the rear MTBD advances past the front MTBD as dynein steps along the microtubule (*19*). Redocking of the linker in the front head would pull on the rear head, causing it to move forward after it dissociates from the microtubule. It is possible that the MTBD of the rear head also swings forward, through a rotation of the ring or a change in the stalk-ring angle, so that it can more easily rebind to a new tubulin binding site toward the microtubule minus end. Information on the relative positions of the ring, stalk/MTBD, and linker in different nucleotide states will help to resolve the sequence of conformational changes that occurs as cytoplasmic dynein steps along the microtubule.

References and Notes

1. R. D. Vale, R. M. Milligan, *Science* **288**, 88 (2000).
2. A. F. Neuwald, L. Aravind, J. L. Spouge, E. V. Koonin, *Genome Res.* **9**, 27 (1999).
3. P. A. Tucker, L. Sallai, *Curr. Opin. Struct. Biol.* **17**, 641 (2007).
4. J. P. Erzberger, J. M. Berger, *Annu. Rev. Biophys. Biomol. Struct.* **35**, 93 (2006).
5. E. J. Enemark, L. Joshua-Tor, *Curr. Opin. Struct. Biol.* **18**, 243 (2008).
6. C. Ulbrich *et al.*, *Cell* **138**, 911 (2009).
7. S. A. Burgess, M. L. Walker, H. Sakakibara, P. J. Knight, K. Oiwa, *Nature* **421**, 715 (2003).
8. A. J. Roberts *et al.*, *Cell* **136**, 485 (2009).
9. M. Samso, M. P. Koonce, *J. Mol. Biol.* **340**, 1059 (2004).
10. B. Wickstead, K. Gull, *Traffic* **8**, 1708 (2007).
11. P. Hook, R. B. Vallee, *J. Cell Sci.* **119**, 4369 (2006).
12. T. Kon, T. Mogami, R. Ohkura, M. Nishiura, K. Sutoh, *Nat. Struct. Mol. Biol.* **12**, 513 (2005).
13. T. Kon, M. Nishiura, R. Ohkura, Y. Y. Toyoshima, K. Sutoh, *Biochemistry* **43**, 11266 (2004).
14. S. L. Reck-Peterson, R. D. Vale, *Proc. Natl. Acad. Sci. U.S.A.* **101**, 1491 (2004).
15. C. Cho, S. L. Reck-Peterson, R. D. Vale, *J. Biol. Chem.* **283**, 25839 (2008).
16. M. A. Gee, J. E. Heuser, R. B. Vallee, *Nature* **390**, 636 (1997).
17. M. P. Koonce, *J. Biol. Chem.* **272**, 19714 (1997).
18. A. P. Carter *et al.*, *Science* **322**, 1691 (2008).
19. S. L. Reck-Peterson *et al.*, *Cell* **126**, 335 (2006).
20. Materials and methods are available as supporting material on *Science* Online.
21. J. M. Davies, A. T. Brunger, W. I. Weis, *Structure* **16**, 715 (2008).
22. A. W. Serohijos, Y. Chen, F. Ding, T. C. Elston, N. V. Dokholyan, *Proc. Natl. Acad. Sci. U.S.A.* **103**, 18540 (2006).
23. M. Rappas *et al.*, *Science* **307**, 1972 (2005).
24. M. N. Fodje *et al.*, *J. Mol. Biol.* **311**, 111 (2001).
25. S. E. Glynn, A. Martin, A. R. Nager, T. A. Baker, R. T. Sauer, *Cell* **139**, 744 (2009).
26. M. Bochtler *et al.*, *Nature* **403**, 800 (2000).
27. D. A. Bushnell, P. Cramer, R. D. Kornberg, *Structure* **9**, R11 (2001).
28. E. J. Enemark, L. Joshua-Tor, *Nature* **442**, 270 (2006).
29. N. D. Thomsen, J. M. Berger, *Cell* **139**, 523 (2009).
30. D. Gai, R. Zhao, D. Li, C. V. Finkielstein, X. S. Chen, *Cell* **119**, 47 (2004).
31. V. L. Grum, D. Li, R. I. MacDonald, A. Mondragon, *Cell* **98**, 523 (1999).
32. S. M. Doyle, S. Wickner, *Trends Biochem. Sci.* **34**, 40 (2009).
33. I. R. Gibbons *et al.*, *J. Biol. Chem.* **280**, 23960 (2005).
34. T. Kon *et al.*, *Nat. Struct. Mol. Biol.* **16**, 325 (2009).
35. J. P. Abrahams, A. G. W. Leslie, R. Lutter, J. E. Walker, *Nature* **370**, 621 (1994).
36. H. Wang, G. Oster, *Nature* **396**, 279 (1998).
37. K. Yamada *et al.*, *Mol. Cell* **10**, 671 (2002).
38. A. Gennerich, R. D. Vale, *Curr. Opin. Cell Biol.* **21**, 59 (2009).
39. N. Kodera, D. Yamamoto, R. Ishikawa, T. Ando, *Nature* **468**, 72 (2010).

40. We thank N. Zhang (UCSF), J. Holton (Advanced Light Source), H. Schmidt (MRC), E. Gleave (MRC), and M. Sirajuddin (UCSF) for their assistance and helpful discussions. This work was supported by the NIH (R.D.V.), Jane Coffin Child Foundation (A.P.C.), Lymphoma and Leukemia Foundation (A.P.C.), American Heart Association (C.C.), and Genentech Graduate Student Fellowship (C.C.). The PDB accession number for this dynein dimer structure is 3QMZ.

Supporting Online Material

www.sciencemag.org/cgi/content/full/science.1202393/DC1
Materials and Methods
Figs. S1 to S7
Table S1
References

3 January 2011; accepted 7 February 2011
Published online 17 February 2011;
10.1126/science.1202393

REPORTS

Synthesis and Measurement of Ultrafast Waveforms from Five Discrete Optical Harmonics

Han-Sung Chan,[1,2]* Zhi-Ming Hsieh,[1]* Wei-Hong Liang,[1] A. H. Kung,[1,2]† Chao-Kuei Lee,[3] Chien-Jen Lai,[4] Ru-Pin Pan,[5] Lung-Han Peng[6]

Achieving the control of light fields in a manner similar in sophistication to the control of electromagnetic fields in the microwave and radiofrequency regimes has been a major challenge in optical physics research. We manipulated the phase and amplitude of five discrete harmonics spanning the blue to mid-infrared frequencies to produce instantaneous optical fields in the shape of square, sawtooth, and subcycle sine and cosine pulses at a repetition rate of 125 terahertz. Furthermore, we developed an all-optical shaper-assisted linear cross-correlation technique to retrieve these fields and thereby verified their shapes and confirmed the critical role of carrier-envelope phase in Fourier synthesis of optical waveforms.

Function generators routinely produce electric fields in the form of sine, sawtooth, square, and triangular waves and even sophisticated arbitrary waveforms in the radio-frequency (RF) regime. These function generators use electronic oscillators whose speed is limited to $\lesssim$100 GHz to obtain the waveforms. Extending the production of similar waveforms to the optical region (10^{15} cycles/s) is of great interest but presents a major challenge (*1*). By manipulating the phases of high-order harmonics generated in an intense laser field, researchers have obtained single-cycle attosecond sine and cosine pulses in the extreme ultraviolet to soft x-ray region (*2*). Alternatively, by spectral (line-by-line) control of individual components of a comb of carrier frequencies, they can produce shaped envelopes that engulf many cycles of a rapidly oscillating optical field and have a high level of complexity and good fidelity (*3*). The challenge that we address here is the realization of instantaneous electric field optical waveforms similar to those obtained with function generators in the RF region and the measurement of these fields.

It is known from Fourier transform theory that periodic waveforms can be synthesized with a series of sine or cosine waves at frequencies starting with the fundamental frequency. When these frequencies span much more than an octave

[1]Institute of Atomic and Molecular Sciences, Academia Sinica, Taipei, Taiwan. [2]Institute of Photonics Technologies, National Tsing Hua University, Hsinchu, Taiwan. [3]Department of Photonics, National Sun Yat Sen University, Kaohsiung, Taiwan. [4]EECS Department, Massachusetts Institute of Technology, Cambridge, MA 02139, USA. [5]Department of Electrophysics, National Chiao Tung University, Hsinchu, Taiwan. [6]Department of Electrical Engineering and Graduate Institute of Photonics and Optoelectronics, National Taiwan University, Taipei, Taiwan.

*These authors contributed equally to this work.
†To whom correspondence should be addressed. E-mail: akung@ee.nthu.edu.tw

in the frequency spectrum, they form a train of subcycle pulses (*4*). For controllable manipulation of these waves, their initial phases must be stable, preferably aligned with each other; the phase slip between the peak of the synthesized field and the peak of the envelope that shrouds the field (the carrier-envelope phase or CEP) should remain constant.

An approach that could satisfy these conditions is to expand the spectrum of a mode-locked Ti:sapphire laser (*5*). Another is to link and phase-lock the spectra of two mode-locked lasers (*6*). However, pulse shapers with a resolution that is sufficiently high to provide octave-spanning line-by-line phase and amplitude control are not available. Another approach is to generate a wide comb of precisely equidistant optical frequencies by nonlinear mixing of phase-coherent laser oscillators, but the complexity of the locking scheme has thus far inhibited realization of this scenario (*4*).

Yet another approach that has demonstrated success in frequency comb generation is molecular modulation (*7*). In this method, two lasers with a frequency difference nearly equal to a molecular vibrational or rotational transition are used to adiabatically drive the molecular ensemble. With H_2 as the molecular medium, an equidistant comb of frequencies has been generated with an overall conversion efficiency of >10%. The spectrum of the generated comb easily covers several octaves (*8*–*11*). Furthermore, by beginning with a driving laser frequency that is nearly equal to the molecular Raman resonance, the frequencies of the comb are commensurate ($\omega_n = n\omega_m$, where ω_m is the modulation frequency). The CEP is then stable and can be controlled precisely at all times (*12*, *13*). With a comb thus generated, the aforementioned conditions for optical waveform synthesis are satisfied, permitting the synthesis of repetitive femtosecond and subfemtosecond optical waveforms of any desired shape.

Here we describe the synthesis of electromagnetic waves whose instantaneous electric fields are shaped to form a train of periodic sawtooth, square, or subcycle cosine and sine pulses. The fields we synthesized are enclosed under a Gaussian envelope of 3.5-ns full-width half-maximum (FWHM), by virtue of the pulsed laser we used to generate the frequencies used in the synthesis. The repetition rate of the pulses in the train is 125 THz, determined by the fundamental frequency, and is equivalent to a period duration of 8.02 fs. The shortest pulse synthesized within each period is a subcycle cosine pulse that has a field FWHM of 834 attoseconds and an intensity envelope FWHM of 1.45 fs. These results manifest a major step toward achieving the optical analog of a RF function generator.

The optical waveforms we synthesized have a multi-octave-spanning spectral width, and as a result are difficult to characterize with often-used ultrafast pulse characterization techniques (*14*). We show here that when the frequencies are commensurate, shaper-assisted cross-correlation can be effectively used to retrieve these fields and thereby verify their successful synthesis. We used the technique to confirm the critical role of CEP in waveform synthesis.

To prepare the harmonic frequency comb, we directed a monochromatic beam of transform-limited linearly polarized pulses 3.5 ns in duration, with its frequency centered at 4155.235 cm^{-1} (~20 mJ/pulse, 15 pulses/s), into a $LiNbO_3$ crystal to generate its second harmonic. Both colors were then used to drive the Q(1) vibrational Raman coherence of room-temperature H_2 at a pressure of 1 bar to produce several higher-order harmonics to form a frequency comb (*13*, *15*). The power of the fundamental and the second harmonic exiting the cell were attenuated by a factor of 3 to avoid optical damage to the spatial light modulators and other optics downstream. The net pulse energies of the first five harmonics generated were 320, 270, 150, 33, and 6.7 μJ (±20% each, ~780 μJ total), respectively, measured just in front of a 200-μm-thick β-barium borate (BBO) crystal that mixes the harmonics to produce heterodyne signals used to adjust the phases and to set the CEP (Fig. 1A). The front face of this β-BBO crystal was where the shaped optical fields were realized and characterized.

When independently controlling the amplitude and the phase of each harmonic, the maximum number of distinguishable wave shapes that can be synthesized with N harmonics is 2^N. Fine variation of these 2^N waveforms is possible subject to the resolution, overall stability, and signal-to-noise ratio. To achieve the highest degree of complexity and fidelity, it is optimal to begin with N as large as possible. Yet simulation shows that commonly used periodic waveforms such as the square, sawtooth, subcycle sine and cosine, and triangle can be synthesized to a good degree of resemblance to the actual waveform with just the fundamental plus the next few harmonics (*16*). Hence, for demonstration purposes, we used the first five harmonics (first to fifth components of the frequency comb) to synthesize optical fields and verify their shapes in this work. The corresponding wavelengths used were nominally 2406, 1203, 802, 602, and 481 nm. With these five harmonics, the frequency comb spectrum extends over two octaves. The shortest pulses they can collectively synthesize are transform-limited subcycle cosine pulses, each spanning 0.75 optical cycle with a temporal field FWHM of 834 attoseconds. A few of the optical field waveforms that could be synthesized with these harmonics are depicted in Fig. 1B. Parameters relevant to their synthesis are tabulated in table S1.

After generating these five harmonics, we set their amplitudes to the desired values. The amplitude of each harmonic was attenuated by a home-built liquid crystal spatial light modulator (LCSLM) that was fabricated as an amplitude modulator. The next major step was to align their phases. Because the comb frequencies are multiples of the fundamental frequency, every harmonic will heterodyne with a signal at the same frequency derived by optically summing two lower harmonics. The resulting interference signal can then be used to align the phases of the comb frequencies and for phase compensation and optimization (*4*, *13*). We followed the alignment procedure described in (*13*). The signal obtained from heterodyning the second harmonic generated from the β-BBO crystal with that from the Raman process was used to establish the CEP. To adjust the phases, we used a LCSLM configured for the task (*15*).

Once the phases are aligned and the amplitudes are set to values required for the desired waveform, the synthesis is complete. A train of pulses of a desired shape is created from the superposition of these harmonics. The instantaneous field of the pulses can be reconstructed from the known amplitudes, the CEP, and the alignment of the relative phases.

We next show that the fields can be measured to verify the waveforms. It has long been

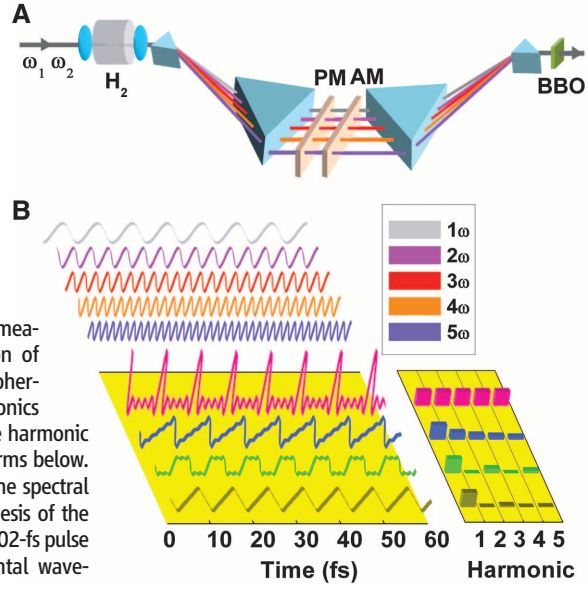

Fig. 1. (**A**) Schematic of the experimental setup to synthesize waveforms using harmonics generated by coherent modulation of the H_2 molecule. ω_1 and ω_2 designate the frequencies of the inputs to the H_2 cell. AM and PM are liquid crystal spatial light modulators (LCSLMs) that, respectively, attenuate the powers (and thus amplitudes) of the harmonics and adjust and compensate their phases. These LCSLMs are also used as pulse shapers for the cross-correlation measurements. (**B**) Pictorial demonstration of ultrafast waveforms obtained by the coherent superposition of the first five harmonics of a fundamental wavelength. The five harmonic waves are depicted above, the waveforms below. The panel on the lower right depicts the spectral field amplitudes required for the synthesis of the respective waveforms on the left. The 8.02-fs pulse spacing originates from a fundamental wavelength of 2406 nm.

established that field retrieval is possible by linear cross-correlation (*17*). The method is seldom used because implementing it requires a reference pulse with an exceptionally broad bandwidth. In the present experiment, the bandwidth of more than two octaves is sufficient for linear cross-correlation to be employed. We used the electronic pulse shaping technique (*18*) to split the synthesized waveform $E(t)$ into a reference pulse waveform $E_I(t)$ to retrieve the field of a target waveform $E_b(t)$, where $E_b(t) = E(t) - E_I(t)$ (*19*). Because of this splitting, 100% retrieval of $E(t)$ is not possible. However, by choosing $E_I(t)$ to be small compared to $E(t)$, one can achieve nearly complete retrieval by this technique. Theoretical justification of this approach and a detailed description of its implementation are given in Materials and Methods of the supporting online material. The value of the relative phases among the harmonics is required in programming the pulse shaper, so these values must be known when implementing electronic pulse splitting for this correlation measurement.

We begin by retrieving the field of a sawtooth waveform. The CEP of a sawtooth waveform is $\pi/2$, which we set at the time of the synthesis. Thus, $E(t) = \{i, i/2, i/3, i/4, i/5\}$. The energies of the first five harmonics were attenuated from their initial values by the amplitude-adjusting LCSLM to 167, 41.7, 18.5, 10.5, and 6.7 μJ per ns pulse, respectively. The total pulse energy of ~244 μJ thus comprises normalized amplitudes (which scale as the square root of energy) of {1, 1/2, 1/3, 1/4, 1/5} for the harmonics, as required by a sawtooth waveform. To perform the cross-correlation, we created a transform-limited subcycle cosine pulse train $E_I(t) = \{1/10, 1/10, 1/10, 1/10, 1/10\}$ and $\phi_{nI} = 0$, $\phi_{ceI} = 0$. The remaining field of the sawtooth then constitutes a second pulse train $E_b(t)$. $E_b(t) = E(t) - E_I(t) = \{i - 1/10, i/2 - 1/10, i/3 - 1/10, i/4 - 1/10, i/5 - 1/10\}$ (in the complex plane). These phasor quantities of $E_I(t)$ and $E_b(t)$ were used to program a pulse shaper to split $E(t)$ into $E_I(t)$ and $E_b(t)$ and set a time delay τ between the two fields. The pulse shaper comprises the same phase and amplitude LCSLMs that were used in the first part of the experiment. Varying τ then produced the cross-correlation of $E_I(t)$ and $E_b(t)$. The cross-correlation signal $I(\tau)$ is the sum of the average power of the harmonics at each delay τ and was measured with a broadband thermopile without dispersing the harmonics, because the waveform materializes only when the harmonics are superimposed in time and space. $I(\tau)$ was then recorded and processed with a PC. Meanwhile, because the $I(\tau)$ measurement is an average power measurement that is insensitive to phase fluctuations, we verified that the CEP and the relative phases of the harmonics remained stable throughout the correlation measurement by measuring the heterodyne signal of the incident harmonics at random time delays during each correlation scan; we thereby ensured that the phases had not drifted and pulse splitting was properly executed so that the observed results could be interpreted correctly.

Histograms of the cross correlation signal taken at each time delay are shown in Fig. 2A. The associated relative-phase information of the incident field extracted from heterodyne measurements is shown in Fig. 2B. The observed changes to the relative phases at various time delays have a cumulative standard deviation of ±0.05π. This phase fluctuation only has a minor effect in distorting the shape of the waveform (fig. S3).

We simulated the cross correlation result using Eq. 1:

$$I(\tau) \propto \sum_n (a_0^2 + b_n^2) + 2a_0 \sum_n b_n \cos(n\omega\tau + n\phi_{bn} + \phi_{ceb}) \quad (1)$$

where a_0 is the amplitude of $E_I(t)$, and b_n, ϕ_{bn}, and ϕ_{ceb} are the amplitudes and the relative phases of the nth component and the CEP of $E_b(t)$. These amplitudes and phases are the normalized phasor quantities of $E_I(t)$ and $E_b(t)$, and their values are based on those of normalized $E(t)$ shown above. The simulation and the measured data are connected by a linear scaling factor and a DC offset, which we obtained by least-squares fitting of the calculated result to the measured data at each delay τ. The fitted factor and offset in turn are

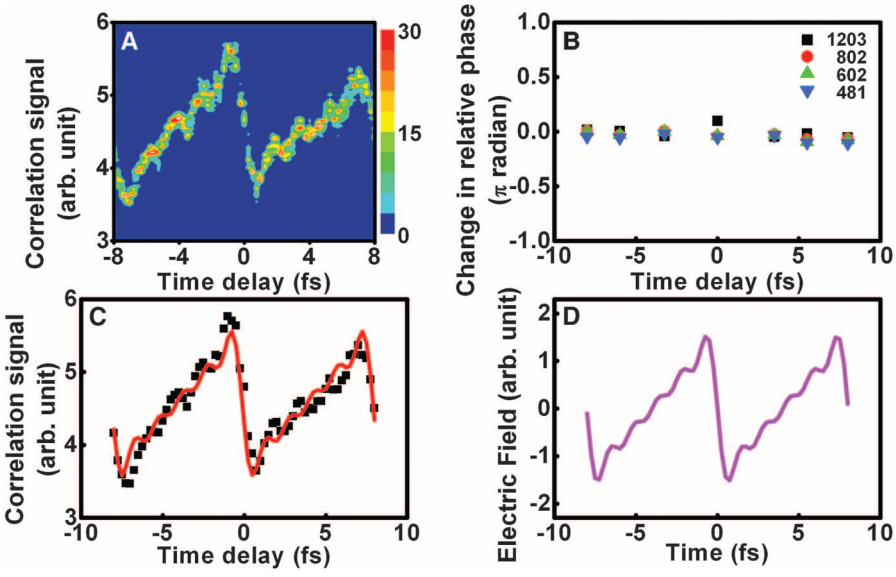

Fig. 2. (**A**) Color-coded histograms of the measured linear cross-correlation signal. A third axis (color scale) represents the frequency of occurrence of the measured signal strength at each time delay. (**B**) Time-averaged fluctuation of the relative phase of the incident harmonics derived from heterodyne signals at each of the harmonics measured at randomly selected time delays and plotted as a change in the relative phase. Each data point is the average of 30 laser shots. (**C**) Numerical simulation (solid red curve) scaled to match the measured correlation data (points). The method of scaling is explained in the text. Each data point is the average of 120 readings of the thermopile meter recording. At zero time delay, the waveform in front of the β-BBO crystal is a sawtooth. This waveform is Fourier reconstructed with the measured CEP and the amplitudes of the five harmonics and is shown in (**D**) for comparison with the signal in (C).

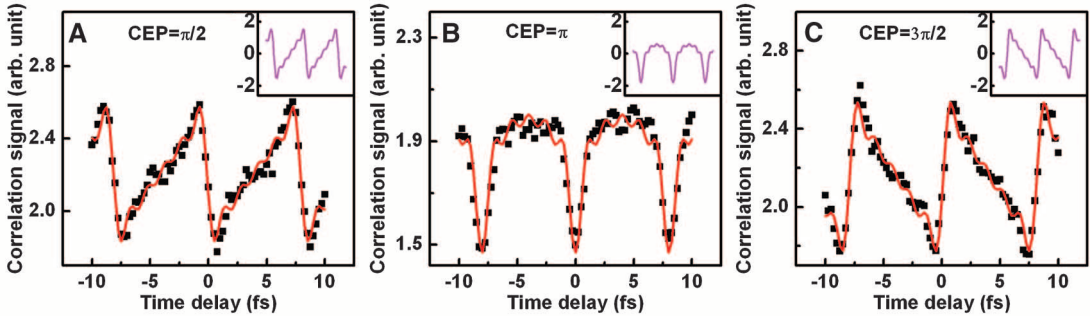

Fig. 3. (**A** to **C**) Evolution of the cross-correlation signal when only the CEP (not harmonic field amplitude) is varied in synthesizing the waveform. The normalized amplitudes are the same as in Fig. 2. The CEP values are shown in the respective panels. These waveforms all have the same envelope, but their instantaneous electric fields as represented by the cross-correlation signal are substantially different, in complete agreement with Fourier Transform theory. The corresponding reconstructed fields are shown in the insets as a reference.

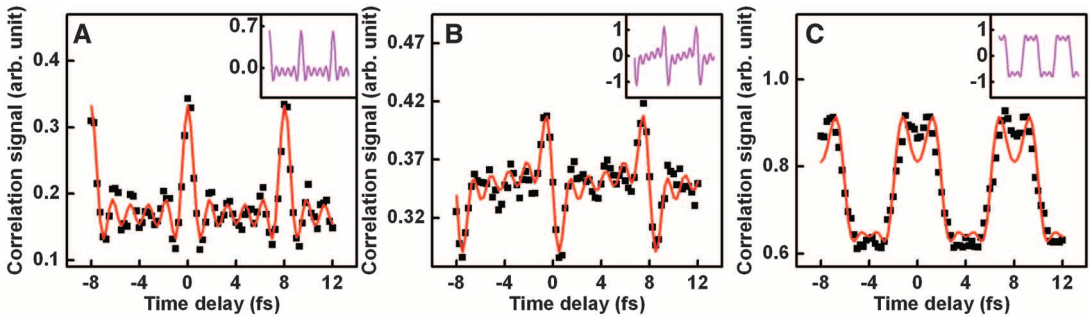

Fig. 4. Cross-correlation signals obtained for a few of the pulse trains shown in Fig. 1B. The amplitudes required for the syntheses are given in table S1: (**A**) transform-limited subcycle cosine (CEP = 0); (**B**) transform-limited subcycle sine (CEP = $\pi/2$); (**C**) square pulses with CEP = 0. The corresponding reconstructed fields are shown in the insets.

used to plot the solid curve in Fig. 2C, which shows good agreement between simulation and experimental data. At zero time delay, the combined $E_I(t)$ and $E_b(t)$ equals $E(t)$, the field of the synthesized sawtooth. This field can be Fourier reconstructed from the CEP and the amplitudes (Fig. 2D). A comparison of Fig. 2, C and D, indicates that the sawtooth field is nearly completely retrieved, thus confirming the efficacy of the shaper-assisted linear cross-correlation technique. Given the many sources that lead to amplitude fluctuations and phase distortions, this result demonstrates the robustness of the synthesized pulses, permitting successful field retrieval.

The instantaneous field of a Fourier-synthesized waveform is CEP dependent, whereas the pulse envelope is not [for an illustration, see figure 3 in (*20*)]. This result can now be experimentally validated here. Using the same sawtooth as an example, we recorded the $I(\tau)$ of waveforms that have identical field amplitudes but different CEPs. The results are shown in Fig. 3, where the waveforms have the same normalized amplitudes as those in Fig. 2 but three different values of the CEP ($\pi/2$, π, and $3\pi/2$). The effect of the CEP on the shape of the electric field as predicted by Fourier analysis is clearly displayed.

The procedure we have described can be extended to synthesize and retrieve various repetitive fields. For example, transform-limited subcycle sine and cosine pulse trains are formed with normalized amplitudes of {1,1,1,1,1} for five harmonics and a CEP of $\pi/2$ and 0, respectively. A square wave has amplitudes of {1, 0, −1/3, 0, 1/5} and a CEP of 0. Cross-correlation of these synthesized fields is shown in Fig. 4.

The average power of the beam of synthesized pulses in this experiment was a few milliwatts. This power is limited mainly by the power of the generated fifth harmonic and the repetition rate of the pump laser. One desirable improvement is to substantially increase the duty cycle of the laser. Raising the pump laser pulse energy and repetition rate, as well as using a larger beam size, could easily increase the average power to the watt level. Starting with a continuous-wave (CW) or quasi-CW laser source could make the synthesized waveforms inherently more stable. Several groups are making substantial progress in this direction (*21*, *22*).

Despite the limited number of waveforms that can be synthesized with five harmonics, we have described a simple solution to an optical waveform synthesizer that is analogous to RF and microwave function generators and showed that several common waveforms are accessible. We further showed an all-optical scheme to retrieve the instantaneous field. For broad application, it is desirable to have many more spectral components available for the synthesis. Other research groups have obtained >200 sidebands by driving the rotational Raman and vibrational Raman coherence simultaneously (*23*).

References and Notes

1. E. Goulielmakis *et al.*, *Science* **317**, 769 (2007).
2. G. Sansone *et al.*, *Science* **314**, 443 (2006).
3. Z. Jiang, C.-B. Huang, D. E. Leaird, A. M. Weiner, *Nat. Photonics* **1**, 463 (2007).
4. T. W. Hansch, *Opt. Commun.* **80**, 71 (1990).
5. L. Matos *et al.*, *Opt. Lett.* **29**, 1683 (2004).
6. R. K. Shelton *et al.*, *Science* **293**, 1286 (2001).
7. S. E. Harris, A. V. Sokolov, *Phys. Rev. Lett.* **81**, 2894 (1998).
8. A. V. Sokolov, D. R. Walker, D. D. Yavuz, G. Y. Yin, S. E. Harris, *Phys. Rev. Lett.* **85**, 562 (2000).
9. J. Q. Liang, M. Katsuragawa, F. L. Kien, K. Hakuta, *Phys. Rev. Lett.* **85**, 2474 (2000).
10. S. W. Huang, W.-J. Chen, A. H. Kung, *Phys. Rev. A* **74**, 063825 (2006).
11. T. Suzuki, M. Hirai, M. Katsuragawa, *Phys. Rev. Lett.* **101**, 243602 (2008).
12. W.-J. Chen *et al.*, *Phys. Rev. Lett.* **100**, 163906 (2008).
13. Z.-M. Hsieh *et al.*, *Phys. Rev. Lett.* **102**, 213902 (2009).
14. D. Keusters *et al.*, *J. Opt. Soc. Am. B* **20**, 2226 (2003).
15. Methods and experimental details are available as supporting material on *Science* Online.
16. See, for example, www.falstad.com/fourier/.
17. A. M. Weiner, in *Ultrafast Optics* (Wiley, New York, 2009), p. 92.
18. A. M. Weiner, *Rev. Sci. Instrum.* **71**, 1929 (2000).
19. A. Galler, T. Feurer, *Appl. Phys. B* **90**, 427 (2008).
20. S. N. Goda, M. Y. Shverdin, D. R. Walker, S. E. Harris, *Opt. Lett.* **30**, 1222 (2005).
21. J. T. Green, J. J. Weber, D. D. Yavuz, *Phys. Rev. A* **82**, 011805(R) (2010).
22. F. Couny, F. Benabid, P. J. Roberts, P. S. Light, M. G. Raymer, *Science* **318**, 1118 (2007).
23. D. D. Yavuz, D. R. Walker, M. Y. Shverdin, G. Y. Yin, S. E. Harris, *Phys. Rev. Lett.* **91**, 233602 (2003).

24. We are indebted to S. E. Harris for inspiring us to work on this project and for his comments during manuscript preparation. We thank S.-Y. Wu, W.-J. Chen, and S.-L. Wang for helpful assistance and S. Goda, F.-G. Yee, C.-B. Huang, and C.-L. Pan for discussions. This work was supported by the Academia Sinica (AS-98-TP-A10) and the National Science Council (NSC 97-2120-M-001-002 and NSC 98-2112-M-001-008-MY3) of Taiwan. R.-P.P. was supported by the National Science Council (NSC 96-2221-E-009-131-MY3) of Taiwan.

Supporting Online Material

www.sciencemag.org/cgi/content/full/science.1198397/DC1
Materials and Methods
Figs. S1 to S3
Table S1
Movie S1

28 September 2010; accepted 11 January 2011
Published online 20 January 2011;
10.1126/science.1198397

Layer-by-Layer Removal of Graphene for Device Patterning

Ayrat Dimiev, Dmitry V. Kosynkin, Alexander Sinitskii, Alexander Slesarev, Zhengzong Sun, James M. Tour*

The patterning of graphene is useful in fabricating electronic devices, but existing methods do not allow control of the number of layers of graphene that are removed. We show that sputter-coating graphene and graphene-like materials with zinc and dissolving the latter with dilute acid removes one graphene layer and leaves the lower layers intact. The method works with the four different types of graphene and graphene-like materials: graphene oxide, chemically converted graphene, chemical vapor–deposited graphene, and micromechanically cleaved ("clear-tape") graphene. On the basis of our data, the top graphene layer is damaged by the sputtering process, and the acid treatment removes the damaged layer of carbon. When used with predesigned zinc patterns, this method can be viewed as lithography that etches the sample with single-atomic-layer resolution.

The electronic properties of graphene (*1*), a two-dimensional (2D) network of sp^2 carbon atoms, can vary as a function of the number of carbon layers in the sample (*2*, *3*). Existing methods for patterning graphene do not allow one to control the number of layers removed (*4*–*7*). Some of them are designed to work with a single existing layer of carbon material (*4*, *5*),